IDENTIFYING SPURIOUS MODES IN RF-MEMS RESONATORS USING PHOTOELASTIC IMAGING

Vikrant J. Gokhale[1,2], and Jason J. Gorman[2]
[1]National Institute of Standards and Technology, Gaithersburg MD, USA
[2]University of Michigan, Ann Arbor MI, USA

ABSTRACT

This paper reports the first use of dynamic photoelastic imaging for identifying in-plane vibration modes in high-frequency MEMS resonators. In a set of width-extensional mode resonators (WE-BARs), we map fundamental width-extensional modes $\omega_{(0,1)}$ and unwanted higher-order spurious length-extensional modes $\omega_{(i,0)}$. In addition, we detect unexpected spurious modes 'ω_x' for all designs that are potentially detrimental due to their proximity to $\omega_{(0,1)}$. We show the dependence of both intended modes and spurious modes on aspect ratio and discuss methods of mitigation for the latter. It is shown that the photoelastic technique is broadly applicable to high-resolution mapping and identification of vibration modes in MEMS resonators.

INTRODUCTION

Microelectromechanical (MEMS) resonators are designed to vibrate efficiently at characteristic resonance frequencies that are dependent on material choice, dimensional design, and boundary conditions. MEMS resonators, like all mechanical structures, can have multiple degrees of freedom, can be made with anisotropic materials, or can be actuated into motion with asymmetric driving forces, using anisotropic transduction mechanisms. These factors can lead to the transduction of several vibration modes and frequencies, both intended and unintended. In applications such as frequency synthesis, communications, and sensing, the goal is almost always to produce vibration at a single well-defined resonance frequency. The presence of multiple resonance modes within a narrow spectral range can be detrimental, often causing signal intermodulation and increasing spectral noise [1]. It is critical to understand the nature and origin of these unwanted 'spurious' modes to suppress them or move them away from the desired resonance mode. Once identified, one of several solutions can be implemented to mitigate these spurious modes, including redesign [2], acoustic reflectors [3], and phononic shields [4].

Not all spurious modes can be reliably predicted *a priori* by analytic methods that simplify the dynamics of the resonator. On the other hand, computational methods can predict numerous modes which are not always measurable in a real device. In many design lifecycles, the most reliable strategy is to use a combination of analytical and computational estimates to design and build the resonator, followed by experimental characterization and numerical fitting with computational models. Experimental characterization should provide the most detailed information about the dynamics of the resonator. However, the most common contemporary electrical characterization techniques provide only spatially-averaged measurements of current or voltage that may obscure the origin of the spurious mode, making it difficult to reduce the effect of spurious modes in future designs. Optical techniques are preferable for spatially-resolved characterization of the dynamics of MEMS resonators, and for the identification of desired and spurious modes. Contemporary optical techniques for imaging vibration are mainly displacement (or velocity) measurement methods such as interferometry [5], laser Doppler vibrometry (LDV) [6], knife-edge modulation [7, 8], or holographic microscopy [9].

This work presents a new imaging technique using the photoelastic effect, where the reflected amplitude of a probe laser is proportional to the dynamic strain at any point on a vibrating resonator. We demonstrate an application of this photoelastic technique by using it to image strain mode shapes for silicon WE-BARs. We show that it is possible to map the strain mode shapes of the desired width-extensional modes, as well as unwanted spurious modes. We discuss the influence of planar aspect ratio (length/width) on the distribution of strain in the device, and the mode spacing between desired and spurious modes. Such characterization is critical for optimizing the exact vibration mode shapes of the as-fabricated width-extensional modes, and eliminating the spurious modes.

EXPERIMENTAL TECHNIQUE

Photoelastic Imaging

The photoelastic technique relies on the stress-induced birefringence in solid materials. In general, non-birefringent materials not under stress have a single-valued refractive index. When there is mechanical stress on the material, (due to mechanical or thermal loads), there is a change in the refractive index of the material. The stress-induced change in refractive index of a material is given by $\Delta n = -(0.5n^3 p_{ij})\Delta\varepsilon_{ij}$, where n is the nominal refractive index of the material, p_{ij} is the photoelastic matrix of the material, and $\Delta\varepsilon_{ij}$ is the change in strain [10]. This phenomenon is utilized in optical fiber sensors [11] and for measuring the intrinsic stress distribution in thin films [12]. We have implemented a dynamic version of this technique that measures the change in refractive index at the vibration frequency. The stress-induced change in refractive index subsequently modulates the reflected power, P_R, of a probe laser beam incident on the surface of the resonator (i.e., $\Delta P_R(\omega) \propto \Delta n(\omega) \propto \Delta\varepsilon_{ij}(\omega)$.) We have demonstrated this technique in the past to map the spatial decay rate of mechanical energy across the tethers of MEMS resonators [13], and to compare efficiency of tether designs [14].

Experimental Setup and Resonator Design

The WE-BARs used in this work are fabricated in the 10 μm thick silicon device layer of a silicon-on-insulator (SOI) wafer. We use an intensity stabilized He-Ne laser to probe the surface of the vibrating WE-BARs, and a 200 MHz or 1400 MHz photodetector to measure the reflected signal. Full details of the test setup, design considerations, and fabrication process are provided in prior work [13-15].

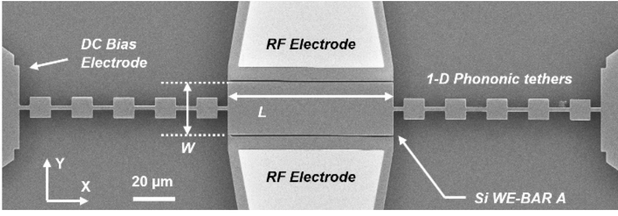

Figure 1: Scanning electron microscope image of a silicon WE-BAR with dimensions 80 µm × 25.5 µm × 10 µm.

We use three WE-BAR designs with varying aspect ratios, as shown in Table I. The expected frequencies for the 1st width-extensional mode for each design are:

$$\frac{\omega_{(0,1)}}{2\pi} = \frac{1}{2w}\sqrt{\frac{E}{\rho}} \qquad (1)$$

Here, E = 160 GPa is the Young's modulus and ρ = 2330 kg·m^{-3} is the mass density of silicon. Similarly, a higher order length-extensional mode for any of the WE-BARs is

$$\frac{\omega_{(i,0)}}{2\pi} = \frac{i}{2l}\sqrt{\frac{E}{\rho}} \qquad (2)$$

Figure 1 shows a scanning electron microscope image of WE-BAR A. All designs presented here have 5-unit 1-dimensional phononic crystal (1D PnC) tethers tailored specifically to confine energy at $\omega_{(0,1)}$, and to provide the highest value of mechanical quality factor (Q) [14].

Table I: WE-BAR Design and Planar Aspect Ratio

WE-BAR	l (µm)	w (µm)	Planar Aspect Ratio (l/w)	Expected Frequency $\omega_{(0,1)}/2\pi$ (MHz)
A	80	25.5	3.13	162
B	75	18.5	4.05	224
C	65	14.5	4.48	286

The WE-BAR under test is mounted on a precision three-axis motion stage with a step resolution of ≈ 10 nm, and the probe laser beam is focused on the top surface. All devices presented here are electrostatically actuated using a 21 V DC bias to the WE-BAR body and an RF signal of 10 mW to both lateral electrodes across a capacitive gap of 500 nm. All measurements are acquired in air.

EXPERIMENTAL RESULTS

For spectral measurements, the probe laser is focused on the geometric center of the WE-BAR, and the reflected signal is measured using the photodetector and a vector network analyzer (VNA). Figure 2 shows a wide spectral scan for WE-BAR A. Three strong mechanical resonances are present in the range of 160 MHz to 170 MHz. Using the precision motion stage and automated LabVIEW control, we scan the WE-BAR under the probe laser and measure the peak reflection amplitude at each step, for each of the three modes. The resulting maps clearly show that the three modes have very different in-plane strain profiles. The insets in Fig. 2 are strain maps corresponding to each spectral peak. Figure 3 shows each map in detail, in comparison with the closest simulated eigenmode. The color range in each strain map shown in this work is scaled to show the maximum range for that data-set. Unless otherwise specified, simulations were carried out using 3D finite element analysis, and show Y-axis strain, $\varepsilon_{yy}(\omega)$.

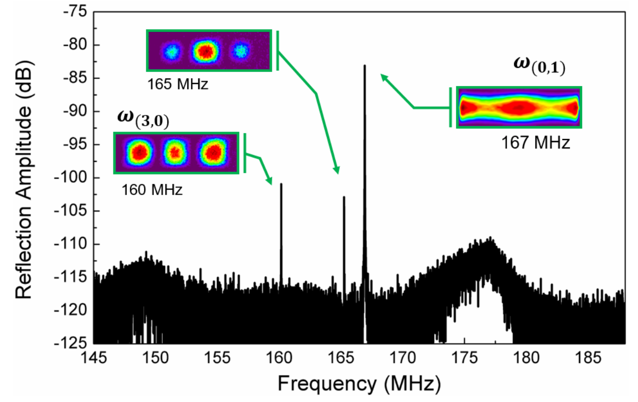

Figure 2: A wide spectral scan for WE-BAR A, acquired using photoelastic modulation, shows the desired and spurious resonant modes. Note that while weaker than the $\omega_{(0,1)}$ mode, both spurious modes have high signal-to-noise ratio, and are close to $\omega_{(0,1)}$. Insets show measured vibrational mode shapes.

The desired width-extensional $\omega_{(0,1)}$ mode at 167 MHz has the highest strain signal. The strain map indicates that the device undergoes axial expansion/compression with displacement along the width dimension. Additional regions of strain situated near the roots of the tether are due to the boundary conditions imposed by the tethers. This is the characteristic fundamental mode shape of a width-extensional mode with finite length.

The two modes at 160 MHz and 165 MHz are unwanted spurious modes that merit further investigation. The strain map for the mode at 160 MHz shows three near-equal regions of strain concentration spaced equally along the length of the WE-BAR. This is the 3rd-order length extensional mode. This mode is transduced since the aspect ratio of WE-BAR A is close to 3, and odd-harmonic length-extensional modes are supported. It is expected that vibration along the length will be significantly damped due to the position and configuration of the tethers and supports of the resonator. This is borne out by the lower peak reflection amplitude for $\omega_{(3,0)}$ relative to $\omega_{(0,1)}$. The measured mode at 165 MHz is an unexpected spurious mode designated as 'ω_x'. A detailed discussion of this ω_x mode is presented in the next section.

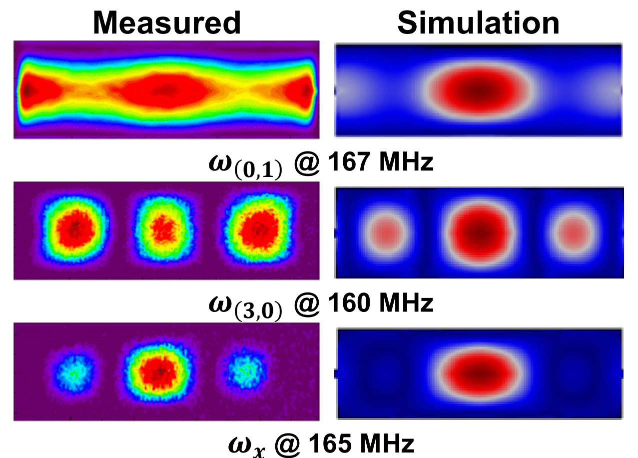

Figure 3: Photoelastic measurements and simulated mode shapes for the in-plane modes of WE-BAR A identified in Fig. 2.

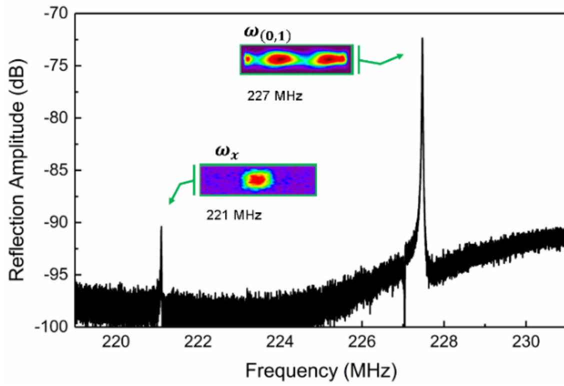

Figure 4: A wide spectral scan for WE-BAR B, shows the desired $\omega_{(0,1)}$ and the spurious ω_x modes clearly. The two modes are spaced only 6 MHz apart. Note the absence of a length-extensional harmonic mode: the aspect ratio of WE-BAR B is close to 4, and even-harmonic length modes will not be supported in the resonant cavity along its length. Insets show vibrational mode shapes. Insets show measured vibrational mode shapes.

Figure 4 shows a wide spectral scan for WE-BAR B, with two clear resonance peaks indicated, and the strain maps shown in the inset. The dominant mode is the $\omega_{(0,1)}$ mode at 227 MHz, with a smaller amplitude for the ω_x mode at 221 MHz. No length-extensional mode is found within this span (or within a broader search range). Since WE-BAR B has an aspect ratio very close to 4, this is expected. Even-harmonic length-extensional modes are not supported. However, the ω_x mode is clearly present, is close to the desired $\omega_{(0,1)}$, and only $\approx$ 18 dB lower in amplitude. Figure 5 compares the measured strain maps with the closest simulated strain eigenmodes. Similarly, WE-BAR C (aspect ratio of 4.48) supports three distinct modes: ω_x at 267 MHz, $\omega_{(0,1)}$ at 282 MHz, and $\omega_{(5,0)}$ at 312 MHz (Fig. 6). Strain maps and corresponding simulated mode shapes that best match the measured data for WE-BAR C are shown in Fig. 7.

DISCUSSION

Some qualitative observations can be made by visually inspecting the strain mode shapes measured using the photoelastic imaging technique. The $\omega_{(0,1)}$ mode shapes for the three designs (as shown in Fig. 3, Fig. 5, and Fig. 7) clearly indicate the effect of aspect ratio on the strain distribution at resonance.

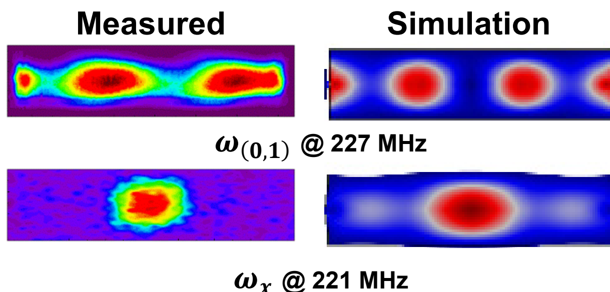

Figure 5: Photoelastic measurements (and simulations) for in-plane strain mode shapes for WE-BAR B identified in Fig. 4. Length-extensional spurious modes were not observed for WE-BAR B. The ω_x mode is still present.

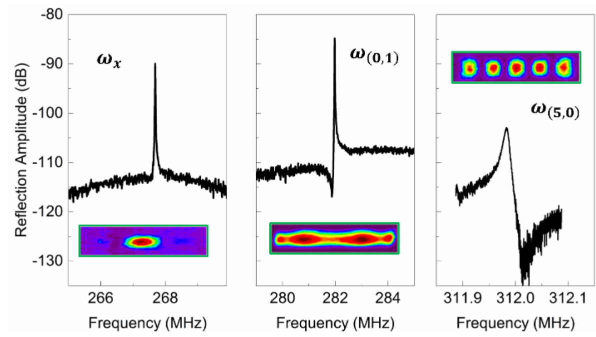

Figure 6: Three resonance modes for WE-BAR C, showing ω_x, $\omega_{(0,1)}$, and $\omega_{(5,0)}$ respectively. The ω_x mode is close to the $\omega_{(0,1)}$ mode, and has comparable reflection amplitude. Insets show measured vibrational mode shapes.

As the (l/w) aspect ratio increases, the strain mode shape evolves with it. The strain tends to distribute more evenly over the resonator length. The odd-harmonic length-extensional modes $\omega_{(3,0)}$ and $\omega_{(5,0)}$ are observed at the expected frequencies, for aspect ratios close to 3 and 5 respectively. For an aspect ratio nearly equal to 4, we do not observe the even-harmonic length-extensional mode.

Preliminary inferences can be drawn about the unexpected ω_x mode. Figure 8 shows the mode spacing between ω_x and $\omega_{(0,1)}$ for all three designs. The modes move closer as the aspect ratio decreases. Simulations for WE-BAR A predict a much wider spacing than that observed in practice. Note that the simulations are meant to illustrate trends, and not optimized to fit measured frequencies. The difference in absolute values could be due to differences in material properties, built-in stress, or fabrication tolerances. Simulated strain mode shapes indicate that the ω_x mode involves three subsections of the resonator moving out of phase with adjoining subsections (see inset of Fig. 8). This mode would be hard to detect electrostatically due to charge integration at the electrode. Nevertheless, it is physically present in the mechanical strain spectrum for all three WE-BARs. It is clearly present close to the main $\omega_{(0,1)}$ mode, and could be a potential source of interference unless attenuated, or moved away from $\omega_{(0,1)}$ by dimensional optimization. Based on the simulation study for WE-BAR A, the mode spacing can be increased by increasing the aspect ratio.

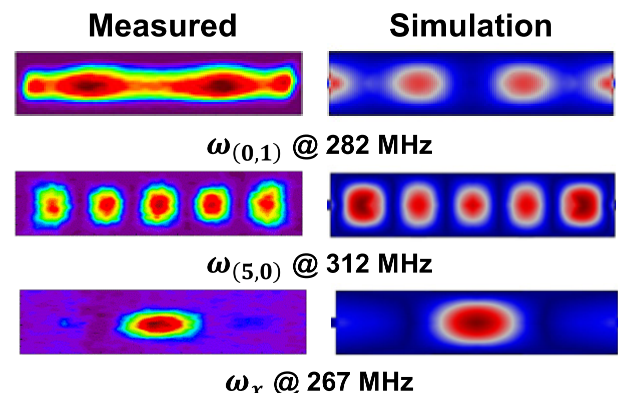

Figure 7: Photoelastic measurements and simulations for in-plane strain mode shapes for WE-BAR C identified in Fig. 6. Note the clearly visible $\omega_{(5,0)}$ and ω_x modes.

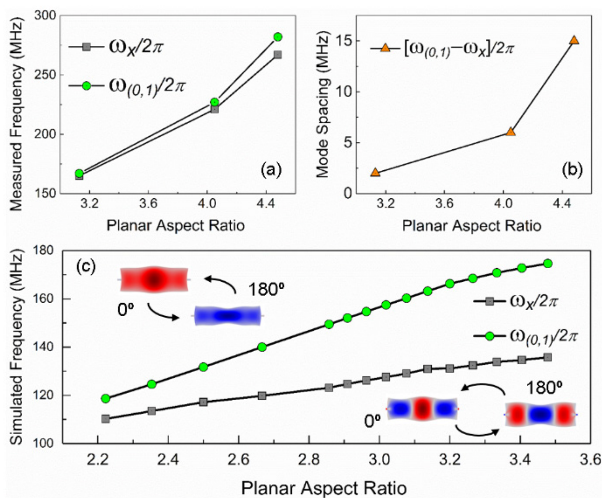

Figure 8: (a) Measured frequencies and (b) mode spacing for the $\omega_{(0,1)}$ and ω_x modes, indicating that the separation between the spurious mode and the desired mode is a function of aspect ratio. (c) Simulation results for the mode spacing for WE-BAR A, as a function of the aspect ratio. Inset denotes both mode shapes. Simulated mode shapes are exaggerated for visual clarity.

CONCLUSION

The photoelastic imaging technique demonstrated here enables the measurement and spatial mapping of dynamic strain in micromechanical structures and devices. This represents a significant addition to contemporary optical metrology techniques that measure displacement. We have shown the utility of this technique in the unambiguous identification of vibration mode shapes in MEMS resonators, and the ability to separate desired and unwanted spurious modes. Further, being able to see and analyze the mode shapes in detail for as-fabricated resonators enables design optimization. Desired vibration modes can be improved by optimizing the spatial strain distibution at resonance. At the same time, unwanted modes can be identified, eliminated, or attenuated, resulting in a cleaner spectral response for the resonator, and fewer constraints on any downstream electronic signal processing.

ACKNOWLEDGMENTS

This research was supported by the NIST, U.S. Department of Commerce Awards 70NANB14H253 and 70NANB16H307.

REFERENCES

[1] H. Zhang, J. Liang, X. Zhou, H. Zhang, D. Zhang, and W. Pang, "Transverse Mode Spurious Resonance Suppression in Lamb Wave MEMS Resonators: Theory, Modeling, and Experiment," *IEEE Transactions on Electron Devices,* vol. 62, pp. 3034-3041, 2015.

[2] T. Makkonen, A. Holappa, J. Ella, and M. M. Salomea, "Finite element simulations of thin-film composite BAW resonators," *IEEE Transactions on Ultrasonics, Ferroelectrics, and Frequency Control,* vol. 48, pp. 1241-1258, 2001.

[3] B. P. Harrington and R. Abdolvand, "In-plane acoustic reflectors for reducing effective anchor loss in lateral–extensional MEMS resonators," *Journal of Micromechanics and Microengineering,* vol. 21, p. 085021, 2011.

[4] S. P. Wang, Laura; Weinstein, Dana, "GAN MEMS Resonator using a folded phononic structure," Hilton Head Island, SC, 2014.

[5] O. Holmgren, K. Kokkonen, T. Veijola, T. Mattila, V. Kaajakari, A. Oja*, et al.*, "Analysis of vibration modes in a micromechanical square-plate resonator," *Journal of Micromechanics and Microengineering,* vol. 19, p. 015028, 2009.

[6] C. Rembe, R. Kant, and R. S. Muller, "Optical Measurement Methods to Study Dynamic Behavior in MEMS," *SPIE,* vol. 4400, 2001.

[7] A. Bosseboeuf, C. Bréluzeau, F. Parrain, P. Coste, J.-P. Gilles, S. Megherbi*, et al.*, "In-plane vibration measurement of microdevices by the knife-edge technique in reflection mode," in *SPIE*, 2006, pp. 63451D-63451D-8.

[8] D. Karabacak, T. Kouh, C. C. Huang, and K. L. Ekinci, "Optical knife-edge technique for nanomechanical displacement detection," *Applied Physics Letters,* vol. 88, p. 193122, 2006.

[9] J. Kühn, T. Colomb, F. Montfort, F. Charrière, Y. Emery, E. Cuche*, et al.*, "Real-time dual-wavelength digital holographic microscopy for MEMS characterization," in *International Symposium on Optomechatronic Technologies*, 2007, p. 10.

[10] L. Shao, M. Zhang, A. Banerjee, P. K. Bhattacharya, and K. P. Pipe, "Electrically driven nanoscale acoustic source based on a two-dimensional electron gas," *Applied Physics Letters,* vol. 103, p. 083102, 2013.

[11] G. Wild and S. Hinckley, "Acousto-Ultrasonic Optical Fiber Sensors: Overview and State-of-the-Art," *IEEE Sensors Journal,* vol. 8, pp. 1184-1193, 2008.

[12] M. Fukuzawa and M. Yamada, "Photoelastic characterization of Si wafers by scanning infrared polariscope," *Journal of Crystal Growth,* vol. 229, pp. 22-25, 2001.

[13] V. J. Gokhale and J. J. Gorman, "Direct measurement of dissipation in phononic crystal and straight tethers for MEMS resonators," in *IEEE MEMS 2017*, Las Vegas, NV, 2017, pp. 958-961.

[14] V. J. Gokhale and J. J. Gorman, "Approaching the intrinsic quality factor limit for micromechanical bulk acoustic resonators using phononic crystal tethers," *Applied Physics Letters,* vol. 111, p. 013501, 2017.

[15] V. J. Gokhale and J. J. Gorman, "Dynamic characterization of in-plane bulk acoustic resonators using high-sensitivity optical reflection measurements," in *Solid-State Sensors, Actuators, and Microsystems Workshop*, Hilton Head Island, SC, 2016, pp. 145-148.

CONTACT

V.J. Gokhale, vikrant.gokhale@nist.gov
J. J. Gorman, gorman@nist.gov